Signal Characteristics of Circular Induction Coil Influenced by Scanning Spatial Location in MFL

by Xiaoming Huang[†], Jianbo Wu[*], Jie Wang[†], Rongbiao Wang[‡], Jian Tang[‡], Yihua Kang[‡], and Hui Fang[†]

ABSTRACT

Accurate evaluation of objects being inspected by the magnetic flux leakage testing (MFL) method relies on a good correlation between the signal characteristics and the discontinuities under actual test conditions. In practical MFL, imperfect shape and position of the products will lead to a changeable spatial location of the sensors and generate different signal characteristics even for the same discontinuity. In this paper, the signal characteristics of the widely used circular induction coil influenced by spatial location are investigated. First, based on magnetic dipole theory, the magnetic flux leakage distribution of a standard discontinuity is obtained. Second, based on Faraday's law of electromagnetic induction, the signal response model of a circular induction coil at an arbitrary spatial location is built. Then, the influence of the coil spatial location on signal characteristics is analyzed by changing the coil spatial location. It is found that the spatial location influences the signal characteristics greatly, including the signal waveform and the amplitude, which should be taken into consideration in the sensor design and signal analysis. Lastly, MFL experiments are conducted to verify the signal characteristics of the circular induction coil, and the testing results are consistent with theoretical analysis.

KEYWORDS: magnetic flux leakage, circular induction coil, signal characteristics, scanning spatial location

* School of Manufacturing Science and Engineering, Sichuan University, Chengdu 610065, China; email wujianbo@scu.edu.cn
† School of Manufacturing Science and Engineering, Sichuan University, Chengdu 610065, China
‡ School of Mechanical Science and Engineering, Huazhong University of Science and Technology, Wuhan 430074, China

Introduction

As a noncontact nondestructive testing (NDT) technology, magnetic flux leakage testing (MFL) is a powerful and highly efficient method that has been widely used for ferromagnetic objects (Kang et al. 2012; Carvalho et al. 2010; Cheng 2016; Zeng et al. 2004; Zhang et al. 2012), such as oil-gas pipeline (Ramuhalli et al. 2003; Sun et al. 2016; API 2008), rail track (Wang et al. 2014), steel wire (Kashyap et al. 2005), oil storage tank bottoms (Cui et al. 2017), and bridge cable (Xu et al. 2012).

Magnetic flux leakage is not affected by the presence of nonferromagnetic media around the specimen, so MFL can still be performed when the surface of the specimen is not clean, such as when the surface has dirt or dust on it (API 2008). The ferromagnetic objects subject to a uniform magnetic field will produce flux leakage if any discontinuities are present in them (Dutta et al. 2009; Li et al. 2007; Mandal and Atherton 1998; Katoh et al. 2003; Al-Naemi et al. 2006). Then, magneto sensors are used to measure the magnetic field around the discontinuity, allowing a quantitative measurement.

Accurate MFL evaluation relies on a good correlation between the signal characteristics and the discontinuity under actual test conditions (Wu et al. 2015). On the one hand, different discontinuity orientations and scanning directions will generate different signal responses, which have been discussed in previous studies (Wu et al. 2015; Wu et al. 2016). On the other hand, under actual inspection conditions, the imperfect shape and position of the products will lead to changeable spatial location of the sensors and generate different signal characteristics even for the same discontinuity, which is the main concern of this paper. In the MFL method, the magneto elements such as hall elements (Ma et al. 2015), giant magneto resistances (Kreutzbruck et al. 2013), and induction coils (Tumanski 2007) are usually used to pick up leaked magnetic fields. Different from the principle of giant magneto resistances and hall elements, with their outputs proportional to the magnetic flux density, induction coils are proportional to the changing rate of magnetic flux, which has high sensitivity and wide bandwidth. Due to these features, induction coils are widely used in MFL. There are two differently shaped induction coils—the line coil and the circular coil—which are used for different requirements. Compared with the line coil, the circular coil has a small sensing area,

which is more sensitive for tiny discontinuities. In automatic inspection, in order to accomplish 100% coverage for the testing objects, the probe needs to be embedded with more circular coils, resulting in more signal channels and a more complicated process system. The signal characteristics of line induction coils affected by sensor arrangement and scanning direction have been investigated (Wu et al. 2016). Until now, there have been few published research studies on signal characteristics influenced by scanning spatial location of the circular induction coil, which is very important for the sensor design (Wade 2012) and signal analysis under actual test conditions.

In this paper, the signal characteristics of the widely used circular induction coil influenced by spatial location are investigated. Based on the magnetic dipole theory, the magnetic flux leakage distribution of a standard discontinuity is obtained, and based on Faraday's law of electromagnetic induction, the signal response model of a circular induction coil at an arbitrary spatial location is built. Magnetic flux leakage signal characteristics in extreme spatial locations are calculated. Then, the influence of the coil spatial location on signal characteristics is analyzed by changing the coil spatial location. MFL experiments are then performed to verify the signal characteristics of the circular induction coil.

Magnetic Flux Leakage Signal Response Model of a Circular Induction Coil

Accurate magnetic flux leakage evaluation relies on a good correlation between the sensor signal characteristics and the discontinuities under actual test conditions. However, under actual test conditions, the imperfect shape and position of the products will lead to a changeable spatial location of the sensors and generate different signal characteristics, even for the same discontinuity. Taking steel pipe inspection as an example, MFL for longitudinal discontinuities of steel pipe on an inspection line is shown in Figure 1, which shows the testing apparatus and the pipe being tested. The steel pipe is driven forward by conveying rollers on the inspection line. When the pipe arrives at the inspection apparatus, it is magnetized by the magnetizer, and then the probes are forced to contact the pipe surface firmly by air cylinders (Wu et al. 2017).

In order to accomplish 100% coverage, the probe is embedded with a coil array, forming a largely effective sensing area, as schematically illustrated in Figure 2. In order to obtain accurate evaluation results, the probe should keep a constant and perfect spatial location with respect to the pipe surface (that is, spatial locations S_1, S_2, and S_3.) All the induction coils have the same lift-off distance from the pipe surface and have their sensing face parallel to the pipe surface. However, under actual test conditions, imperfect shape and position of the pipes will lead to a changeable spatial location of the sensors. The imperfect linearity and roundness of the steel pipe will cause different spatial locations, such as spatial locations S_4, S_5, S_6, and S_7. Besides, the imperfect installation of the conveying rollers will also cause the long pipe to pass by the probe with changeable relative positions. Of course, different spatial locations of the sensors will generate different signal responses even for the same discontinuity, leading to low detection accuracy.

In order to investigate the influence of the spatial location on signal characteristics of the circular induction coil, an analysis model for a circular induction coil was built, as schematically illustrated in Figure 3. A circular induction coil with random spatial location scans a discontinuity in a steel plate; r is the radius of the circular coil; (x_0, y_0, z_0) is the center coordinate of the circular coil; γ is the plane of the circular coil; α is the angle between the X-axis and the
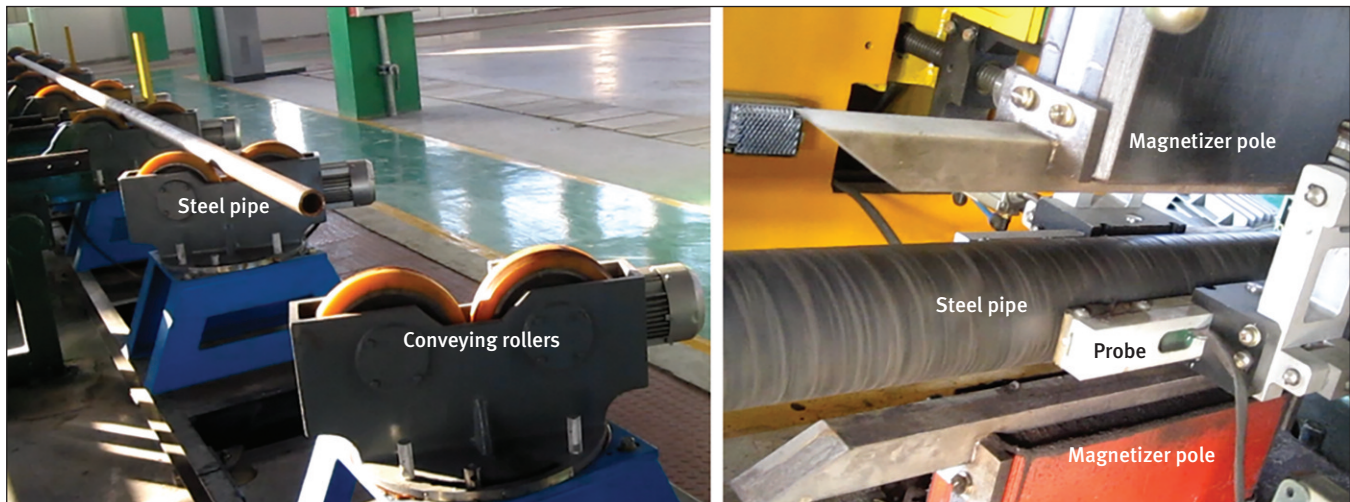

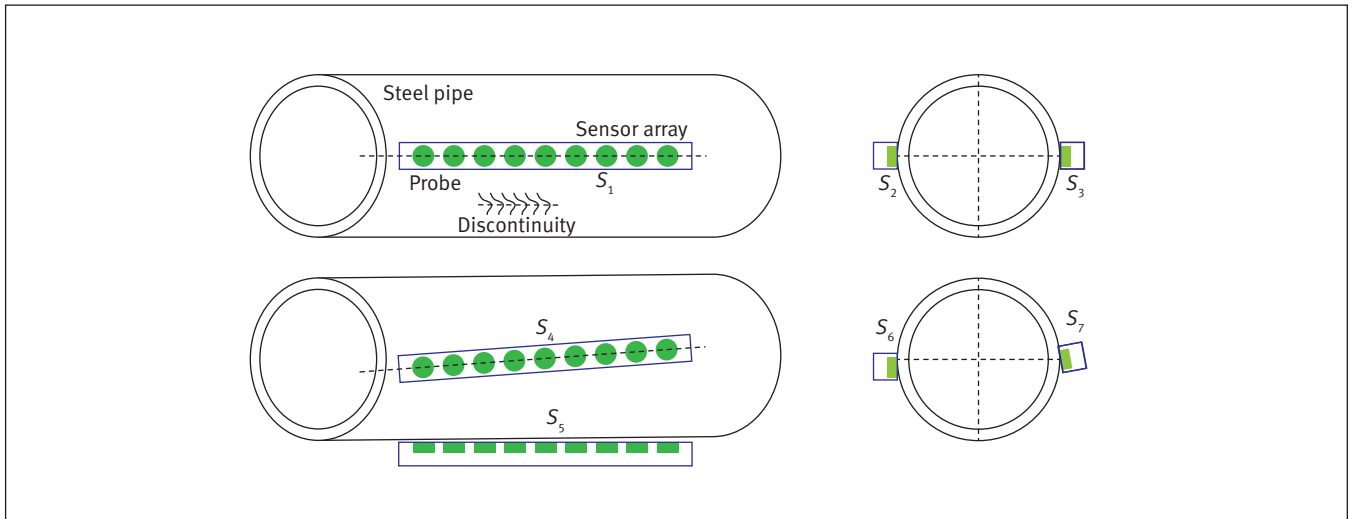**Figure 1. Two views of the MFL inspection apparatus for steel pipes.**

Figure 2. The changeable spatial locations of the probe caused by the imperfect shape and position of the pipes.
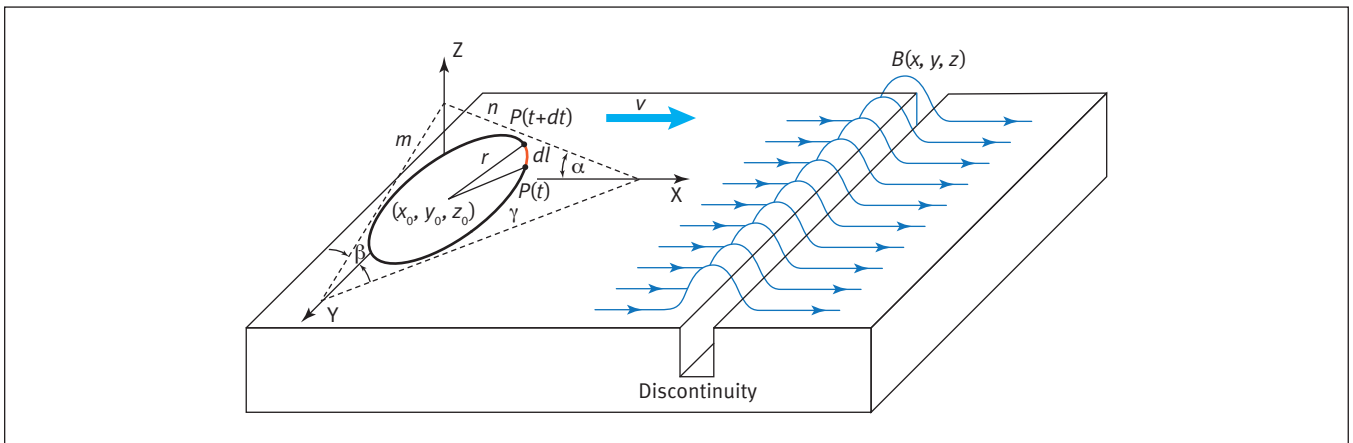

Figure 3. The circular coil with random scanning spatial location.

intersecting line n of the γ plane and XZ plane; and β is the angle between the Y-axis and the intersecting line m of the γ plane and YZ plane. The direction of the scanning velocity v is parallel with the X-axis. The discontinuity orientation is parallel with the Y-axis. When the steel plate is magnetized by an X-axis–oriented magnetization field, magnetic flux leakage $B(x, y, z)$ is generated with its y component $B_y = 0$.

When the circular coil scans above the discontinuity, the magnetic flux leakage will produce induced electromotive force in the coil. Compared to the longitudinal discontinuity, the circular coil has a small sensing area and the y component of the magnetic flux leakage is zero, hence, a two-dimensional discontinuity was used to investigate the signal characteristics of the circular coil, as schematically illustrated in Figure 4. The width and depth of the discontinuity are $2b$ and d, respectively. Opposite magnetic polarities with the density of σ_{ms} are caused on the walls of the rectangle
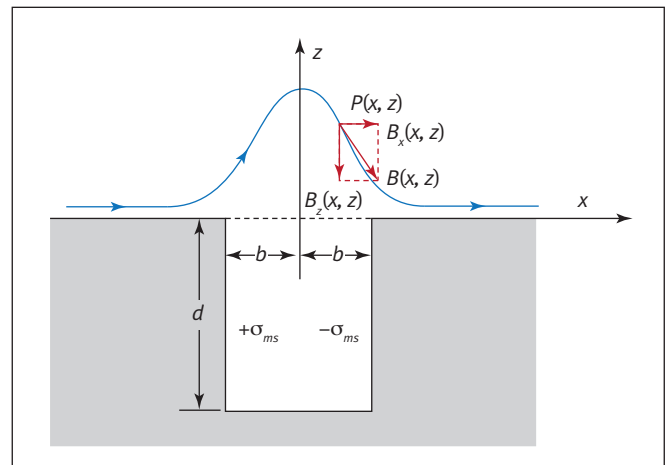

Figure 4. The MFL distribution of the perpendicular discontinuity and its decomposition.

(Mandache and Clapham 2003). The coordinate of the discussed point P is (x, z). The magnetic flux leakage vector $\vec{B}(x, z)$ can be divided up into x component $\vec{B}_x(x, z)$ and z component $\vec{B}_z(x, z)$, as follows:

(1) $$\vec{B}(x,z) = \vec{B}_x(x,z) + \vec{B}_z(x,z)$$

Based on the magnetic dipole model (Zatsepin and Shcherbinin 1966; Shcherbinin and Pashagin 1972; Bray and Stanley 1966), by applying vector superposition and integral operation, the $\vec{B}_x(x, z)$ and $\vec{B}_z(x, z)$ (Shi 2015) can be calculated as follows:

(2) $$\vec{B}_x = \frac{\sigma_{ms}}{2\pi\mu_0} \left[\arctan\frac{d(x+b)}{(x+b)^2 + z(z+d)} - \arctan\frac{d(x-b)}{(x-b)^2 + z(z+d)} \right]$$

(3) $$\vec{B}_z = \frac{\sigma_{ms}}{4\pi\mu_0} \ln \frac{\left([x+b]^2 + [z+d]^2\right)\left([x-b]^2 + z^2\right)}{\left([x-b]^2 + [z+d]^2\right)\left([x+b]^2 + z^2\right)}$$

where

   μ_0 denotes the air permeability, and
   σ_{ms} denotes the magnetic charge density of the perpendicular discontinuity.

To get the magnetic flux leakage distribution of the discontinuity, the width $2b$, the depth d, the lift-off value z, and $\sigma_{ms}/4\pi\mu_0$ are assumed to be 0.5 mm, 0.75 mm, 0.45 mm, and 1 mm, respectively. Along the X-axis from –4.0 mm to 4.0 mm, based on Equations 2 and 3, the x component B_x and the z component B_z are calculated, as displayed in Figure 5. It can be seen that the B_x is an even function with the largest amplitude in the center; in contrast, the B_z is an odd function with the sharpest gradient in the center.
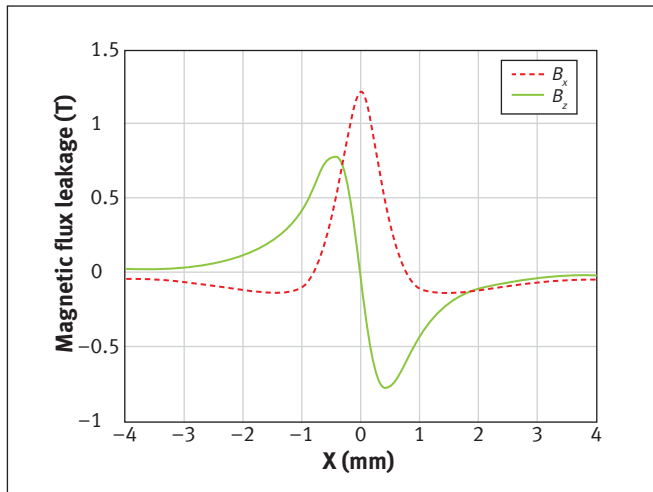

Figure 5. The B_x and B_z of the perpendicular discontinuity.

As displayed in Figure 3, according to Faraday's law of induction, the induced electromotive force of the differential line segment dl is expressed as follows:

(4) $$e_{dl} = \vec{v} \times \vec{B}_{dl} \cdot dl_{\text{effective}}$$

where

   e_{dl} is the induced electromotive force,
   $\vec{v}$ is the velocity vector,
   $\vec{B}_{dl}$ is the magnetic field vector, and
   $dl_{\text{effective}}$ is the effective length of the differential line segment in the velocity direction.

Further, by applying vector decomposition, the induced electromotive force e_{dl} can be expressed as follows:

(5) $$e_{dl} = \vec{v} \times \vec{B}_{dl} \cdot dl_{\text{effective}} = v \cdot B_{dlz} \cdot dl_y$$

where

   B_{dlz} is the Z-axis projection of $\vec{B}_{dl}$, and
   dl_y is the effective length of the differential line segment in the velocity direction.

The direction vectors of intersection line n and m are $\vec{a}$ $(-\cos\alpha, 0, \sin\alpha)$ and $\vec{b}\,(0, -\cos\beta, \sin\beta)$, respectively. The vector of the coil center is $\vec{c}\,(x_0, y_0, z_0)$. Then the coordinate of the point on the coil can be expressed as

(6) $$\vec{p} = \vec{a}u + \vec{b}v + \vec{c}$$

where

   u and v are parameters.

The vector from the coil center to point P is

(7) $$\vec{p} - \vec{c} = \vec{a}u + \vec{b}v$$

The point P is on the circular coil, so the modulus of the vector $|\vec{p} - \vec{c}| = r$. Supposing that $u = w\sin t$, $v = w\cos t$. The vector can be solved by $\vec{p} = \vec{a}\,w\sin t + \vec{b}w\cos t + \vec{c}$. And, the coordinate of any point P on the circular is $\vec{p} = (x_0 - \cos\alpha w\sin t, y_0 - \cos\beta w\cos t, z_0 + \sin\alpha\sin t + \sin\beta w\cos t)$. For the differential line segment dl:

(8) $$B_{dlz} = B_z(P_x, P_z)$$
$$= B_z\left(x_0 - \cos\alpha w\sin t, z_0 + \sin\alpha\sin t + \sin\beta w\cos t\right)$$

$$dl_y = \left(P[t+dt] - P[t+dt]\right)_y$$

Finally, the induced electromotive force e for the entail circular coil can be solved by integration as follows:

(9) $$e = v \cdot \int_0^{2\pi} B_z \begin{pmatrix} x_0 - \cos\alpha w\sin t, z_0 \\ + \sin\alpha\sin t + \sin\beta w\cos t \end{pmatrix} \cdot \begin{pmatrix} P[t+dt] \\ - P[t] \end{pmatrix}_y$$

From Equation 9, the conclusion can be obtained that the sensor spatial location parameters, angles α and β, will influence the signal characteristics. The circular coil with different scanning spatial locations will generate different detection signals even for the same discontinuity, which will seriously affect the detection accuracy. Besides that, the lift-off distances and the scanning velocity will also have an impact on signal characteristics.

Magnetic Flux Leakage Signal Characteristics in Extreme Spatial Locations

Figure 6 shows the three extreme scanning spatial locations of the circular coil above the steel plate's surface. When $\alpha = 0°$, $\beta = 0°$, the coil is in the XY plane and parallel to the surface of the plate, which is a typical arrangement of the circular coil, namely, the horizontal coil. Based on Equations 3 and 9, the
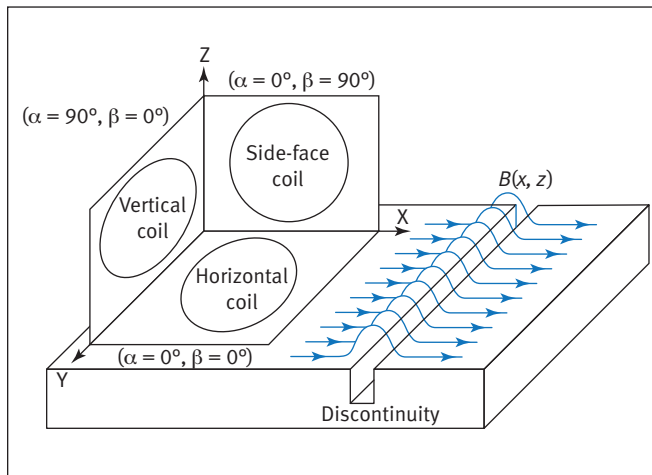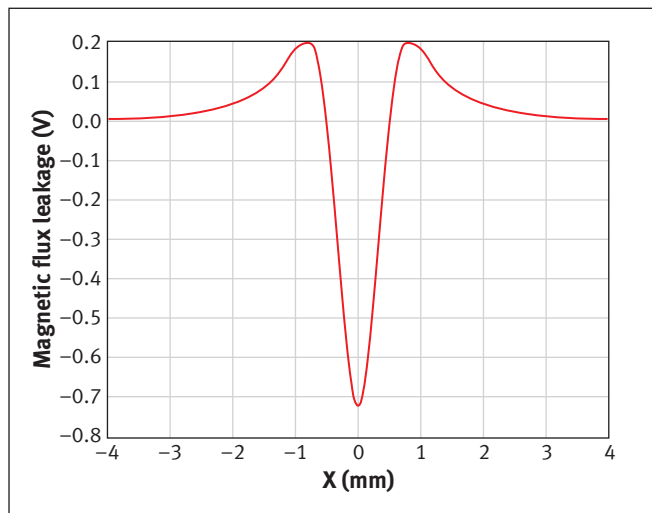
induced electromotive force of the horizontal coil can be expressed as follows:

$$(10) \qquad e = v \cdot \int_0^{2\pi} B_z\left(x_0 - w\sin t, z_0\right) \cdot \left(P[t+dt] - P[t]\right)_y$$

Using the standard discontinuity parameters, the output signal waveform of the horizontal circular coil can be obtained, as shown in Figure 7. It can be noticed that the signal waveform of the horizontal coil is similar with the x component of magnetic flux leakage, which is an even function centered on the discontinuity. It shows the basic waveform characteristic of the output signal of the horizontal coil, which should be taken into consideration in signal post-processing.

When $\alpha = 90°$, $\beta = 0°$, the coil is in the YZ plane and vertical to the surface of the specimen, which is another typical arrangement of the circular coil, namely, the vertical coil. Based on Equations 3 and 9, the output induced electromotive force of the vertical coil can be calculated:

$$(11) \qquad e = v \cdot \int_0^{2\pi} B_z\left(x_0, z_0 + \sin t\right) \cdot \left(P[t+dt] - P[t]\right)_y$$

Similarly, using the standard discontinuity parameters, the output signal waveform of the vertical coil can be obtained as shown in Figure 8. It can be known that the signal characteristic of the vertical coil is greatly different from that of the horizontal coil, which is an odd function similar with the z component of magnetic flux leakage. Comparing Figure 7 and Figure 8, it also can be seen that the two circular coils generate completely different signal waveforms for the same discontinuity; that is, the horizontal coil signal manifests itself in an even function signal wave, and, in contrast, the vertical coil signal is characterized by an odd function signal one.

When $\alpha = 0°$, $\beta = 90°$, the coil is in the side-face; that is, in the XZ plane. In this spatial location, there is no cutting motion, and based on Faraday's law of induction, no induced
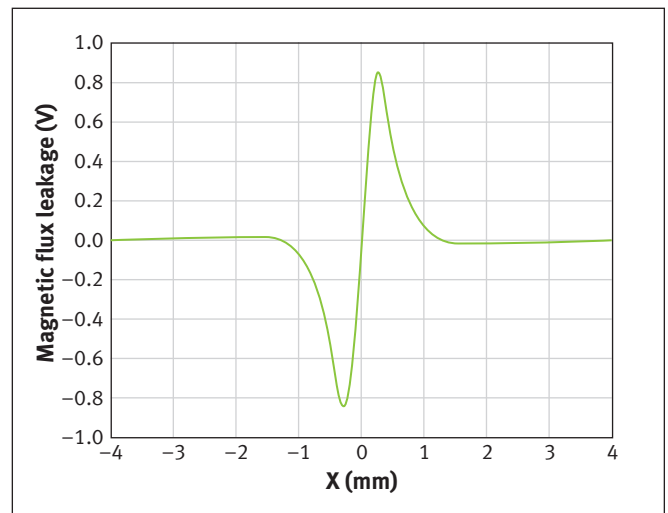

Figure 6. The three extreme spatial locations of the circular coil.

Figure 7. The signal waveform of the horizontal circular coil.

Figure 8. The signal waveform of the vertical circular coil.

electromotive will be generated in the coil. It can be concluded that the side-face scanning spatial location will cause misdetection problems, which should be avoided in MFL.

The Influence of the Scanning Spatial Location on Magnetic Flux Leakage Signal Characteristics

In this section, the influence of the scanning spatial location on signal characteristics is analyzed in the following four aspects: (1) the spatial location with the coil center fixed; (2) the spatial location with different lift-off distances; (3) the spatial location with the lowest point fixed; and (4) the spatial location with different scanning velocities.

The Spatial Location with the Coil Center Fixed

In automatic inspection, imperfect shape and position of the products will lead to a changeable spatial location of the sensors and generate different signal characteristics. In order to analyze the angles α and β alone, the spatial locations are considered with the coil center fixed. The output signals of the circular coil with the spatial location changing from the horizontal location to the vertical location, from the horizontal location to the side-face location, and from the vertical location to the side-face location are calculated, respectively. Based on the Equations 3 and 9, along the X-axis from −2.0 mm to 2.0 mm, with a constant velocity $v = 0.1$ m/s,
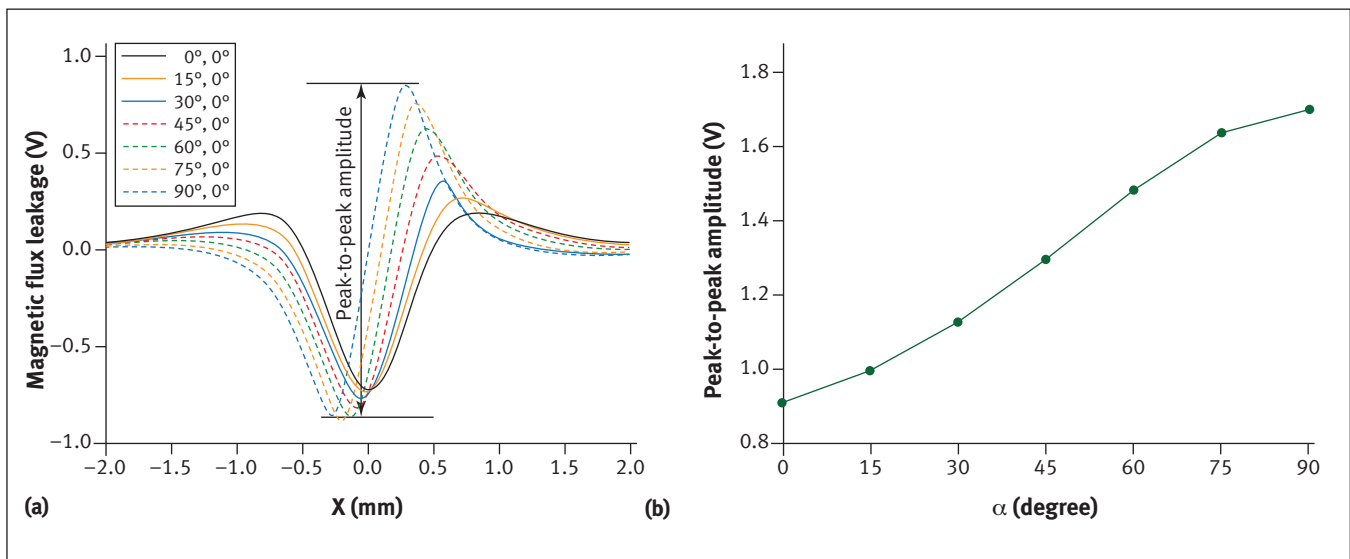

Figure 9. The signal characteristics of the circular coil changing from the horizontal location to vertical one: (a) the signal waveforms; and (b) the signal peak-to-peak amplitude.
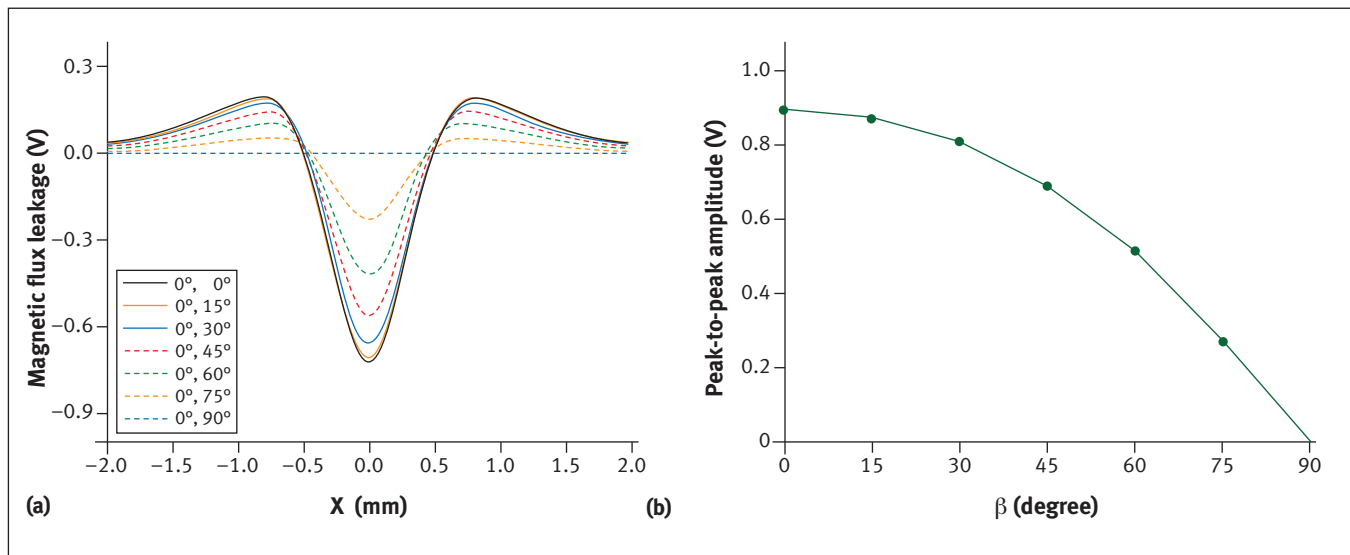

Figure 10. The signal characteristics of the circular coil changing from the horizontal location to the side-face one: (a) the signal waveforms; and (b) the signal peak-to-peak amplitude.

the output signal waveforms are calculated and plotted in Figures 9, 10, and 11 for the same discontinuity.

From Figures 9, 10, and 11, it is found that the spatial location (angles α and β) influences the signal characteristics greatly, including the signal waveform and the amplitude. In order to quantitatively investigate signal amplitude, the peak-to-peak amplitude of the magnetic flux leakage signal is analyzed, as defined in Figure 9, which can eliminate the baseline drift (Wu et al. 2017). From Figure 9, it can be seen that, as the scanning spatial location changes from a horizontal location to a vertical one, the signal waveform manifests itself from an even function wave to an odd one, and the peak-to-peak amplitude increases greatly. From Figure 10, it can be concluded that from the horizontal location to the side-face one, the waveform is always characterized by an odd function and the peak-to-peak amplitude decreases to zero. From Figure 11, it can be seen that the signal waveform

manifests itself from an odd function wave to an even one and the peak-to-peak amplitude decreases greatly with the circular coil changing from the vertical location to the side-face one.

The Spatial Location with Different Lift-Off Distances
In order to get the influence of the coil lift-off distances on magnetic flux leakage sensitivity, the angles α and β are set as five specific values. The same standard discontinuity parameters are used. Based on Equations 3 and 9, the peak-to-peak amplitude of the output signal can be calculated with different lift-off distances z of 0.35 mm, 0.45 mm, 0.55 mm, 0.65 mm, 0.75 mm, 0.85 mm, and 0.95 mm, respectively, as shown in Table 1 and Figure 12.

From Figure 12, it is shown that the peak-to-peak amplitude of the signal gradually decreases with the lift-off distance increasing, since the magnetic flux leakage intensity decreases at a higher lift-off location. Besides, for different angles α and
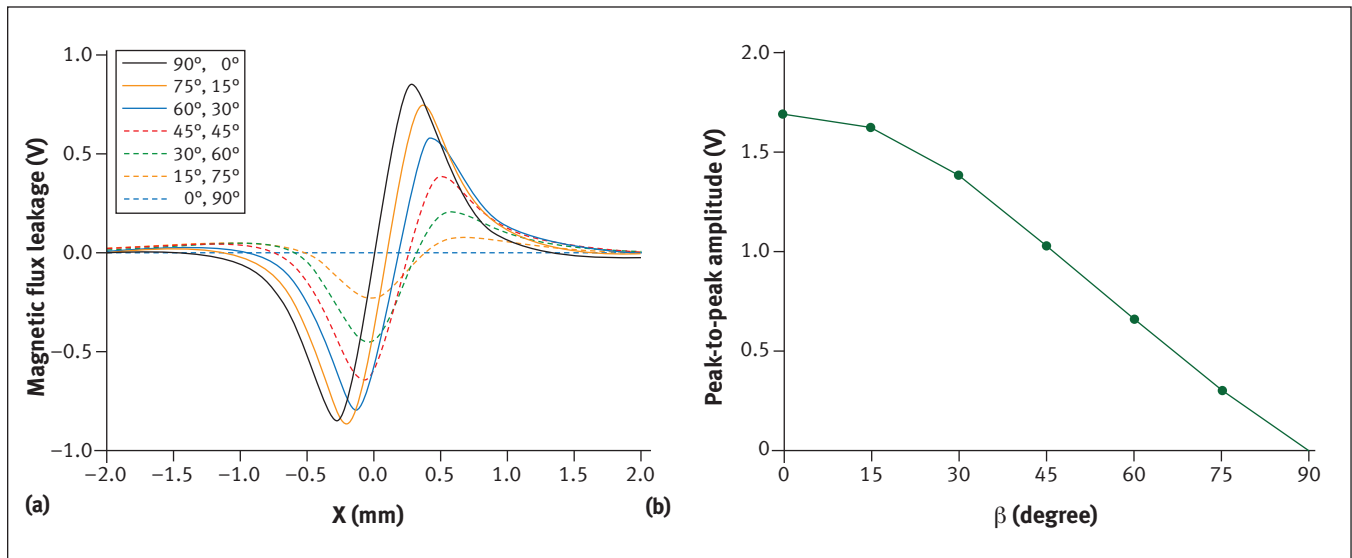

Figure 11. The signal characteristics of the circular coil changing from the vertical location to the side-face one: (a) the signal waveforms; and (b) the signal peak-to-peak amplitude.

TABLE 1
Peak-to-peak amplitude of the circular coil at different lift-off distances

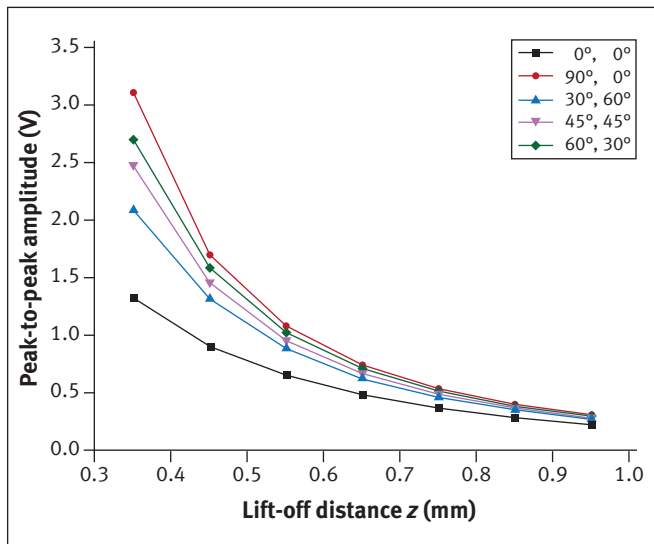| Lift-off z (mm)	Peak-to-peak amplitude $\alpha = 0°, \beta = 0°$	Peak-to-peak amplitude $\alpha = 90°, \beta = 0°$	Peak-to-peak amplitude $\alpha = 30°, \beta = 60°$	Peak-to-peak amplitude $\alpha = 45°, \beta = 45°$	Peak-to-peak amplitude $\alpha = 60°, \beta = 30°$
0.35	1.3251	3.1160	2.0903	2.4823	2.7001
0.45	0.9161	1.7024	1.3183	1.4617	1.5894
0.55	0.6566	1.0848	0.8882	0.9617	1.0251
0.65	0.4854	0.7444	0.6287	0.6728	0.7102
0.75	0.3691	0.5366	0.4626	0.4913	0.5150
0.85	0.2876	0.4010	0.3517	0.3706	0.3864
0.95	0.2273	0.3084	0.2728	0.2871	0.2984

Figure 12. The signal peak-to-peak amplitude of the circular coil at different lift-off distances.

β the declining rate of the amplitude is different. The sensitivity of the horizontal coil ($\alpha = 0°$, $\beta = 0°$) has the lowest declining trend while the sensitivity of the vertical coil ($\alpha = 90°$, $\beta = 0°$) has the fastest one. Therefore, for sensor design, in order to obtain higher sensitivity, the sensors should be placed as close as possible to the object.

The Spatial Location with the Lowest Point Fixed

According to lift-off effect displayed in Figure 12, in order to get a higher sensitivity, the sensors are usually arranged as closely as possible to the object surface. Here, the sensitivity of the typical horizontal coil and vertical coil are analyzed. In the discussion, the two coils have the same lowest point P with a lift-off value of 0.45 mm, as illustrated in Figure 13. To analyze the sensitivity changing rule, the coil spatial location is
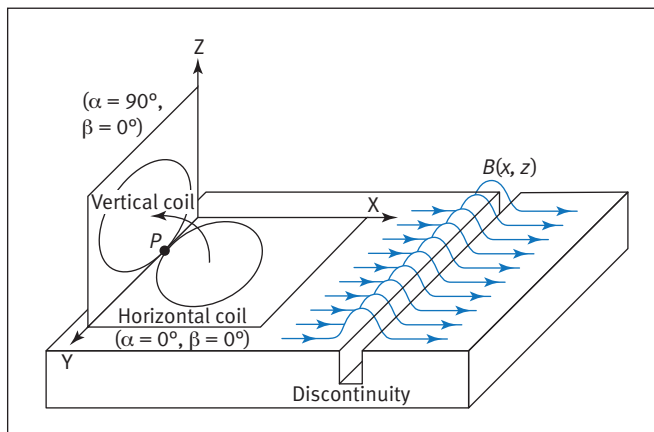

Figure 13. The circular coil rotating around the lowest point.

changed from the horizontal position to vertical with the lowest point P fixed.

Based on Equations 3 and 9, along the X axis from −2.0 mm to 2.0 mm, at different spatial locations, the output signal waveforms are calculated and plotted in Figure 14.

From Figure 14, it can be seen that with the same lowest point, the horizontal coil and vertical coil generate totally different signal characteristics, including the signal waveform and the sensitivity. With the lowest point P fixed, the signal waveform changes from an even function wave to an odd function when the coil scanning spatial location changes from the horizontal position to the vertical one. Besides, it also can be observed that the peak-to-peak amplitude of the signal is gradually reducing. That is to say, with the same lowest point the horizontal coil has a much higher sensitivity than that of the vertical coil, which is a preferable arrangement technique in sensor design.
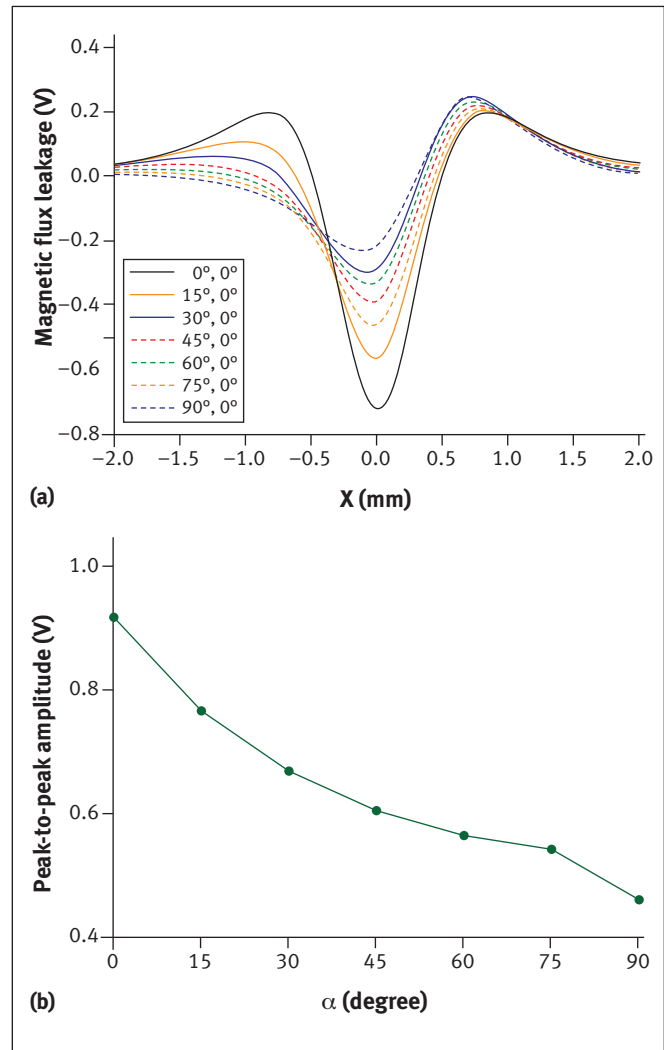

(a)

(b)

Figure 14. The signal characteristics of the circular coil at a fixed lowest point: (a) the signal waveforms; (b) the signal peak-to-peak amplitude.

Peak-to-peak amplitude of the circular coil at different scanning velocities

Scanning velocity v (m/s)	Peak-to-peak amplitude $\alpha = 0°, \beta = 0°$	Peak-to-peak amplitude $\alpha = 90°, \beta = 0°$	Peak-to-peak amplitude $\alpha = 30°, \beta = 60°$	Peak-to-peak amplitude $\alpha = 45°, \beta = 45°$	Peak-to-peak amplitude $\alpha = 60°, \beta = 30°$
0.02	0.18322	0.3404	0.26381	0.2924	0.3179
0.04	0.3664	0.6810	0.5275	0.5847	0.6358
0.06	0.5497	1.0214	0.7913	0.8770	0.9536
0.08	0.7329	1.3618	1.0551	1.1693	1.2715
0.10	0.9161	1.7024	1.3139	1.4617	1.5894

The Spatial Location with Different Scanning Velocities

In order to get the influence of the scanning velocity on magnetic flux leakage sensitivity, the angles α and β are set as five specific values. The same standard discontinuity parameters are used. Based on Equations 3 and 9, the
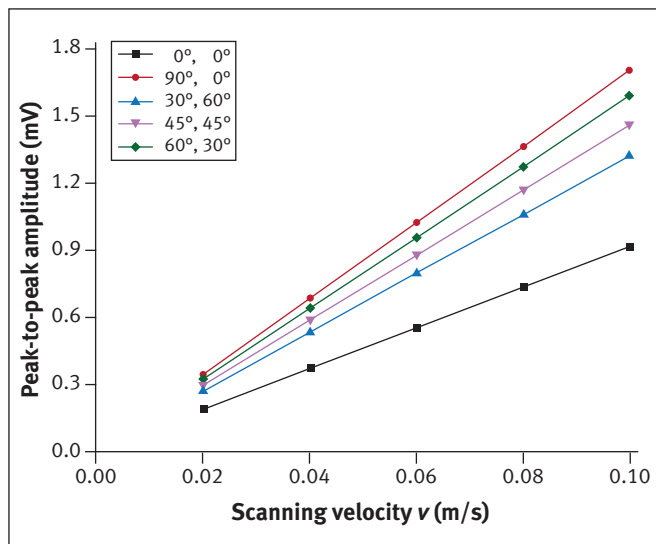

Figure 15. The signal peak-to-peak amplitude of the circular coil at different scanning velocities.

peak-to-peak amplitude of the output signal can be calculated with different scanning velocities v of 0.02, 0.04, 0.06, 0.08, and 0.10 m/s, as shown in Table 2 and Figure 15.

From Figure 15, the conclusion can be made as the velocity v increases, the peak-to-peak amplitude of the signal increases proportionally. Besides, for different angles α and β, the ascending rate of the amplitude is different. The sensitivity of the horizontal coil ($\alpha = 0°, \beta = 0°$) has the lowest ascending trend, while the sensitivity of the vertical coil ($\alpha = 90°, \beta = 0°$) has the fastest one. Therefore, in order to avoid the sensitivity difference caused by velocity change, the MFL inspection should be performed with a stable scanning velocity.

Experiment

Lastly, MFL experiments were conducted to verify the signal characteristics of the circular induction coil. A steel plate (length = 1000.0 mm, width = 150.0 mm, and thickness = 8.0 mm) with a discontinuity was tested by MFL instruments, as shown in Figure 16. A direct current magnetizer was used to generate an axial magnetization field to magnetize the steel plate. A discontinuity (length = 20.0 mm, width = 1.0 mm, and depth = 1.0 mm) was made in the steel plate by a computer numerical controlled (CNC) milling machine. The orientation of the discontinuity is perpendicular to the magnetization direction. It is known that when the MFL is performed at high speed,
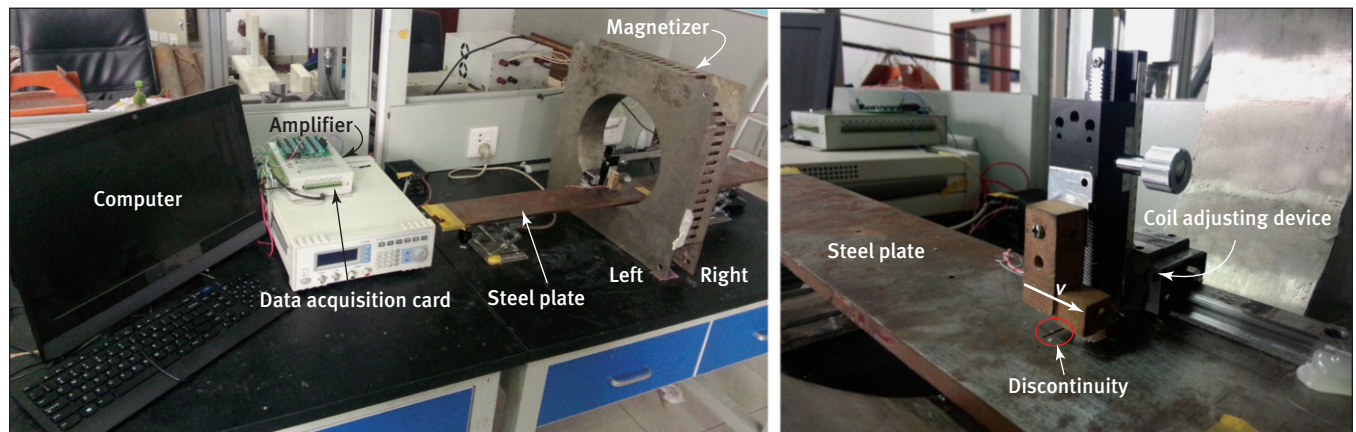

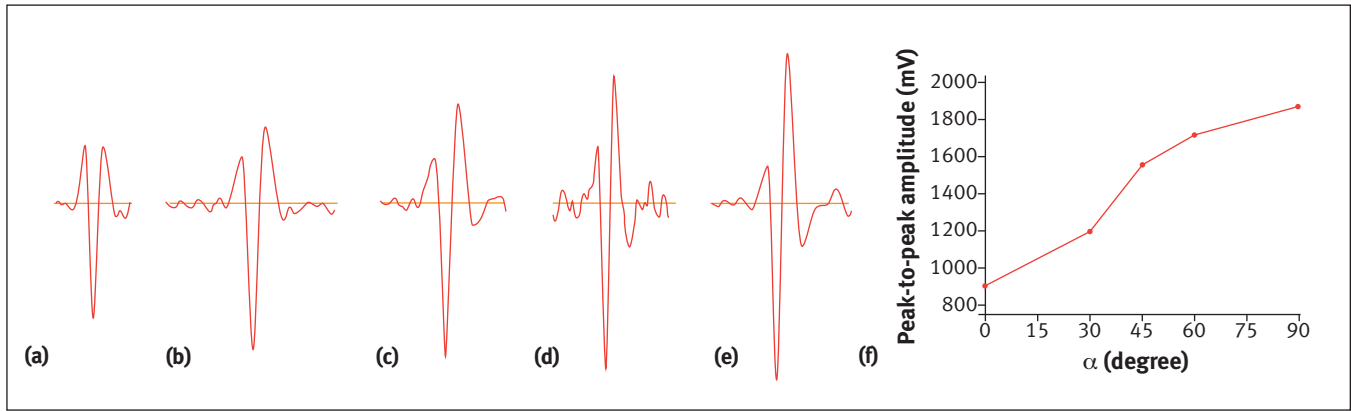**Figure 16. Two views of the MFL instruments for steel plate testing.**

Figure 17. The signals with the circular coil changing from horizontal position to vertical one: (a) α = 0°, β = 0°; (b) α = 30°, β = 0°; (c) α = 45°, β = 0°; (d) α = 60°, β = 0°; (e) α = 90°, β = 0°; and (f) peak-to-peak amplitude.
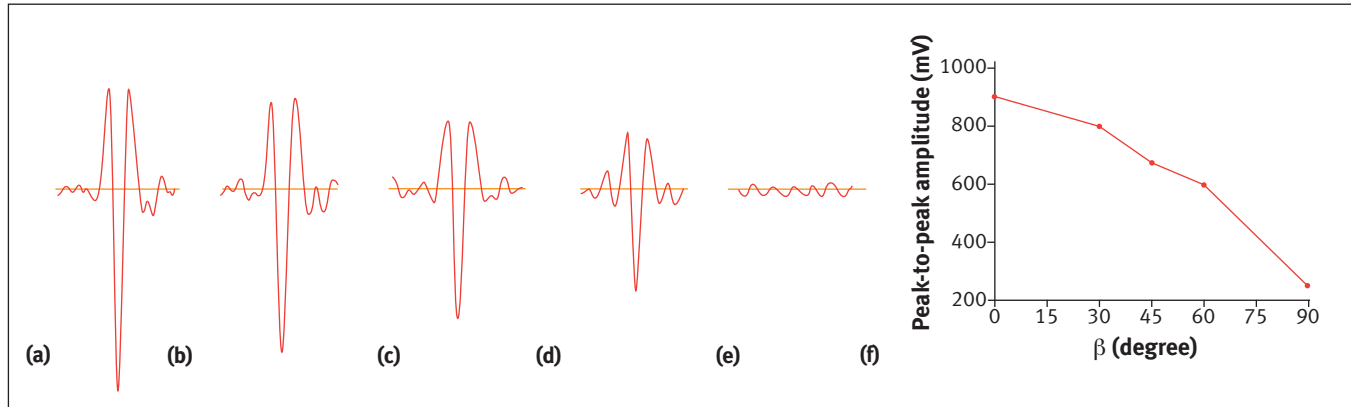
Figure 18. The signals with the circular coil changing from horizontal position to the side-face: (a) α = 0°, β = 0°; (b) α = 30°, β = 0°; (c) α = 45°, β = 0°; (d) α = 60°, β = 0°; (e) α = 90°, β = 0°; and (f) peak-to-peak amplitude.

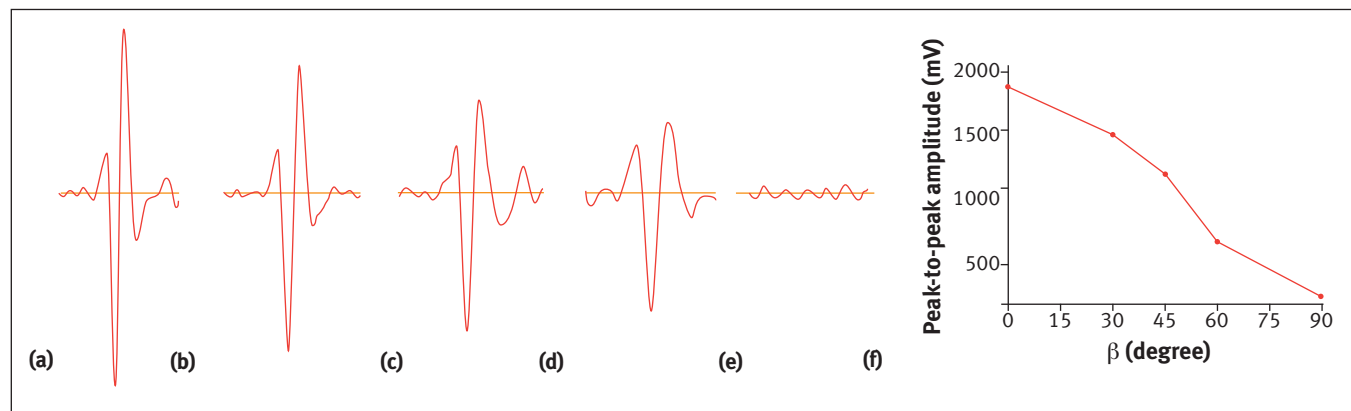

Figure 19. The signals with the circular coil changing from vertical position to the side-face: (a) α = 0°, β = 0°; (b) α = 30°, β = 0°; (c) α = 45°, β = 0°; (d) α = 60°, β = 0°; (e) α = 90°, β = 0°; and (f) peak-to-peak amplitude.

an eddy current effect (Park and Park 2004; Wu et al. 2017) will happen and further influence the magnetization status of the specimen. In this paper, the focus is on signal characteristics of the coil influenced by scanning spatial location. In order to avoid the high-speed eddy current effect, the magnetizer and the steel plate are kept still, and only the coil is driven forward with a fixed velocity v along the axial direction from the left side to right side above the steel plate. Hence, just like the analysis model shown in Figure 3, the scanning direction is parallel to the magnetization direction while they are both perpendicular to the discontinuity orientation. When the coil arrives at the discontinuity location, the magnetic flux leakage will be picked up by a circular coil (radius: 2.5 mm; number of turns: 150). The analog signals from the coil are processed by an amplifier, then collected by a data collector and transformed into digital signals. Finally, the data are stored and analyzed by a computer. In order to analyze the

influence of the different spatial locations, a coil adjusting device is used to adjust the spatial location as required.

In the first study, keeping the center of the coil at the fixed lift-off distance of 4.0 mm, the signal characteristics of the coil with different spatial locations were investigated, as displayed in Figures 17, 18, and 19. From Figure 17, it can be seen that the horizontal coil ($\alpha = 0°$, $\beta = 0°$) and vertical coil ($\alpha = 90°$, $\beta = 0°$) generate different signal waveforms, which matches well with the theoretical analysis results shown in Figures 7 and 8. In addition, when the coil spatial location changes from the horizontal position to vertical, the horizontal position to side-face, and the vertical position to side-face, the signal characteristics change with the same tendency as the theoretical results, including the signal waveform and amplitude. The peak-to-peak amplitude is defined in Figure 17e. In the amplitude discussion, for each spatial location, the defect was tested for 25 times when the sensitivity difference was smaller than 0.5 db, which is the averaged value of the 25 amplitudes used as the analysis data.

Then, the lift-off effect was investigated by placing the coil with its center at different lift-off distances of 3.5, 4.0, 4.5, 5.0, 5.5, 6.0, and 6.5 mm, respectively. Based on Figure 12, the circular coil at the five specific spatial locations were tested. Figure 20 shows the signal amplitude changing trends with the scanning velocity increasing. The conclusion can be reached that the sensitivity increases with the lift-off distance increasing, and that the horizontal coil ($\alpha = 0°$, $\beta = 0°$) sensitivity has the slowest declining trend while the sensitivity of the vertical coil ($\alpha = 90°$, $\beta = 0°$) has the fastest one, which matches the theoretical analysis well shown in Figure 12. Therefore, for sensor design, in order to obtain a higher sensitivity, the sensors should be placed as closely as possible to the object.

Further, keeping the lowest point of the coil at the fixed lift-off distance of 1.0 mm, the signal characteristics of the horizontal and vertical coils were investigated. With the coil changing from the horizontal position to vertical, the typical output signals were picked up, as displayed in Figure 21.
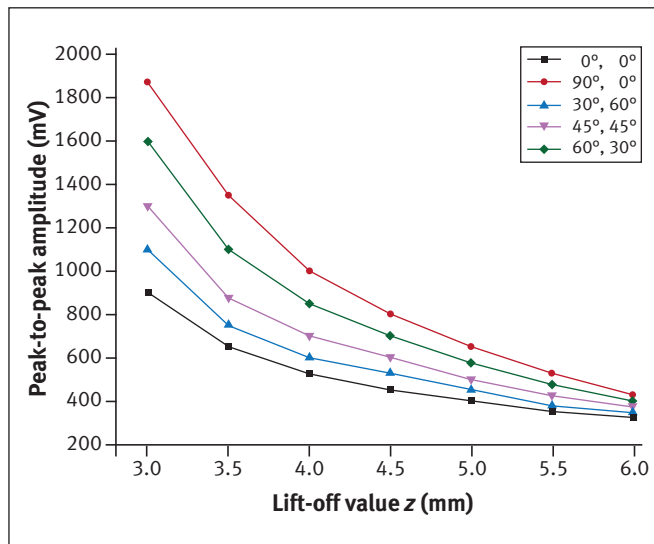

Figure 20. The signal amplitude influenced by lift-off distance.

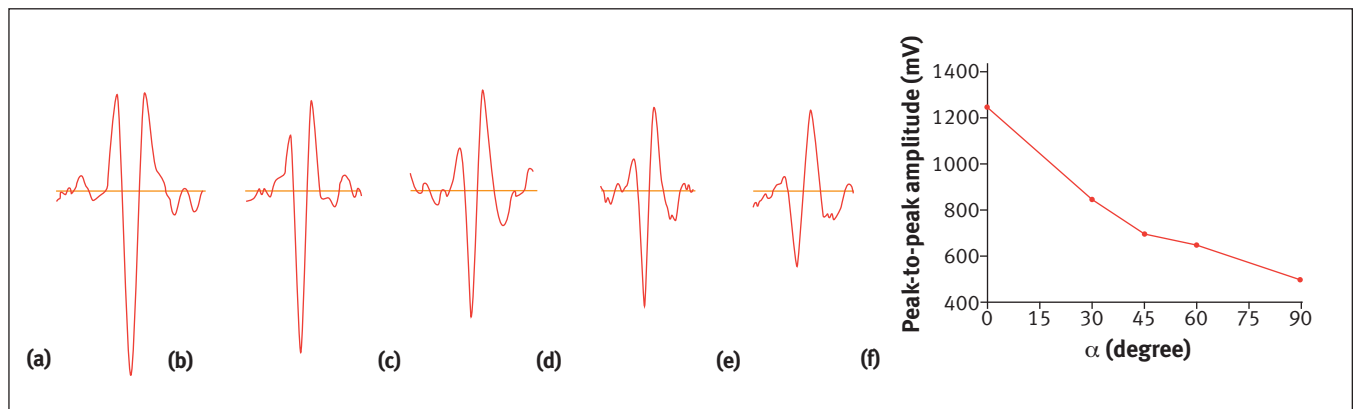**Figure 21. The signals for the circular coil at a fixed lowest point with different spatial locations: (a) $\alpha = 0°$, $\beta = 0°$; (b) $\alpha = 30°$, $\beta = 0°$; (c) $\alpha = 45°$, $\beta = 0°$; (d) $\alpha = 60°$, $\beta = 0°$; (e) $\alpha = 90°$, $\beta = 0°$; and (f) peak-to-peak amplitude.**

It is clear that the horizontal coil has a much higher sensitivity than the vertical coil. Hence, the horizontal position is a preferable coil arrangement technique when the lowest point is fixed, which is consistent with the theoretical conclusion.

Lastly, the effect of the scanning velocity was investigated by performing the coil with different scanning velocities of 0.02, 0.04, 0.06, 0.08, and 0.10 m/s. Based on Figure 15, the circular coil at the five specific spatial locations was tested. Figure 22 shows the signal amplitude changing trends with the scanning velocity increasing. The conclusion can be reached that the sensitivity increases proportionally with the scanning velocity, and that the horizontal coil (α = 0°, β = 0°) sensitivity has the slowest ascending trend while the sensitivity of the vertical coil (α = 90°, β = 0°) has the fastest one, which matches the theoretical analysis well shown in Figure 15. Therefore, in order to avoid the sensitivity difference caused by velocity change, the MFL inspection should be performed with a stable scanning velocity.
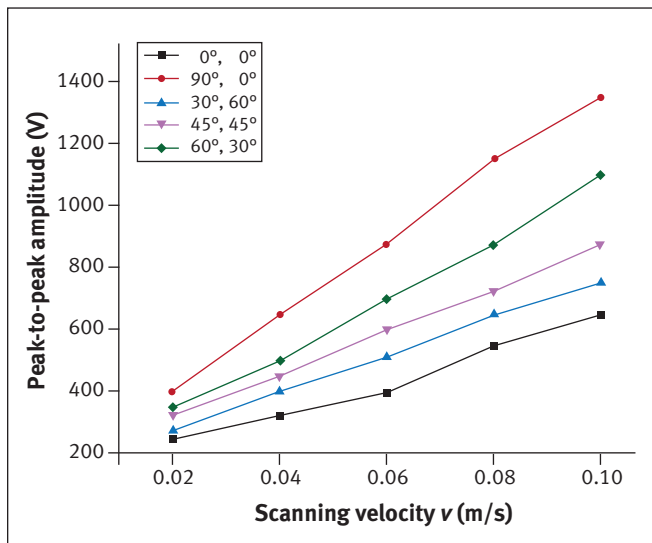

Figure 22. The signal amplitude influenced by scanning velocity.

Conclusions

In this paper, with consideration of actual inspection conditions, in order to improve the accuracy of MFL, the signal characteristics of the widely used circular induction coil influenced by spatial location is analyzed. Based on the magnetic dipole theory and Faraday's law of induction, the signal response model of a circular induction coil at an arbitrary spatial location is set up, and then the influence of coil spatial location is investigated, which is verified by MFL experiments. The conclusions are as follows:

● The horizontal coil signal characteristics are greatly different from the vertical one in that the signal waveform of the horizontal coil is similar with the x component of magnetic flux

leakage, which is an even function centered on the discontinuity; in contrast, the signal waveform of the vertical one has the same changing trend with the z component of magnetic flux leakage, which should be taken into consideration in the signal post-processing.

● The scanning spatial location has a great influence on the signal characteristics, including the waveform and amplitude. Therefore, the coil should keep a constant scanning spatial location in the detection process, which should be considered in the probe design. Besides, the horizontal coil has a higher sensitivity than that of the vertical one when they have the same lowest point, which can provide a theoretical guidance for sensors design. Additionally, placing the sensor as close as possible to the object and performing the inspection with a stable scanning velocity will improve the MFL sensitivity and accuracy.

REFERENCES

Al-Naemi, F.I., J.P. Hall, and A.J. Moses, 2006, "FEM Modelling Techniques of Magnetic Flux Leakage-Type NDT for Ferromagnetic Plate Inspections," *Journal of Magnetism and Magnetic Materials*, Vol. 304, No. 2, pp. e790–e793.

API, 2008, "Specification 6D/ISO 14313: Petroleum and Natural Gas Industries- Pipeline Transportation Systems – Pipeline Valves, Specification for Line Pipe," American Petroleum Institute, Washington, DC, Technical Report 44.

Bray, D. E., and R. K. Stanley, 1966, *Nondestructive Evaluation: A Tool in Design, Manufacturing and Service*, CRC Press Inc., Boca Raton, Florida.

Carvalho, A.A., R.R. Silva, J.M.A. Rebello, and L.V.S. Sagrilo, 2010, "Pattern Recognition Techniques Applied to the Detection and Classification of Welding Defects by Magnetic Testing," *Research in Nondestructive Evaluation*, Vol. 21, No. 2, pp. 91–111.

Cheng, W.Y., 2016, "Magnetic Flux Leakage Testing of Reverse Side Wall-Thinning by Using Very Low Strength Magnetization," *Journal of Nondestructive Evaluation*, Vol. 35, No. 31, doi: 10.1007/s10921-016-0347-7.

Cui, W., H.-Y. Xing, M.-Z. Jiang, and J.-C. Leng, 2017, "Using a New Magnetic Flux Leakage Method to Detect Tank Bottom Weld Defects," *The Open Petroleum Engineering Journal*, Vol. 10, pp. 73–81.

Dutta, S.M., F.H. Ghorbel, and R.K. Stanley, 2009, "Simulation and Analysis of 3-D Magnetic Flux Leakage," *IEEE Transactions on Magnetics*, Vol. 45, No. 4, pp. 1966–1972.

Fernandes, B., J.D. Wade, D.K. Nims, and V.K. Devabhaktuni, 2012, "A New Magnetic Sensor Concept for Nondestructive Evaluation of Deteriorated Prestressing Strand," *Research in Nondestructive Evaluation*, Vol. 23, No. 1, pp. 46–68.

Kang, Y.H., J.B. Wu, and Y. H. Sun, 2012, "The Use of Magnetic Flux Leakage Testing Method and Apparatus for Steel Pipe," *Materials Evaluation*, Vol. 70, No. 7, pp. 821–827.

Kashyap, S. K., G. Laxminarayna, S. Tewari, and A. Sinha, 2005, "Non-Destructive Testing of Steel Wire Ropes and Their Discard Criteria," *Proceedings of the 8th International Conference on Non-Destructive Testing in Engineering*, Portorož, Slovenia, September 2005, pp. 1–3.

Katoh, M., N. Masumoto, K. Nishio, and T. Yamaguchi, 2003, "Modeling of the Yoke-Magnetization in MFL – Testing by Finite Elements," *NDT & E International*, Vol. 36, No. 7, pp. 479–486.

Kreutzbruck, M., M. Pelkner, T. Erthner, and V. Reimund, 2013, "A6.3 - Automated Non-Destructive Testing of Roller Bearings Using GMR-Sensorarrays," *Proceedings SENSOR 2013*, AMA Conferences 2013, Nürnberg, Germany, 14–16 May 2013, pp. 138–142.

Li, Y., J. Wilson, and G.Y. Tian, 2007, "Experiment and Simulation Study of 3D Magnetic Field Sensing for Magnetic Flux Leakage Defect Characterisation," *NDT & E International*, Vol. 40, No. 2, pp. 179–184.

Ma, Y., R. He, and J. Chen, 2015, "A Method for Improving SNR of Drill Pipe Leakage Flux Testing Signals by Means of Magnetic Concentrating Effect," *IEEE Transactions on Magnetics*, Vol. 51, No. 9, doi: 10.1109/TMAG.2015.2427272.

Mandal, K., and D.L. Atherton, 1998, "A Study of Magnetic Flux-Leakage Signals," *Journal of Physics D: Applied Physics*, Vol. 31, No. 22, pp. 3211–3217.

Mandache, C., and L. Clapham, 2003, "A Model for Magnetic Flux Leakage Signal Predictions," *Journal of Physics D: Applied Physics*, Vol. 36, No. 20, pp. 2427–2431(5).

Park, G.S., and S.H. Park, 2004, "Analysis of the Velocity-Induced Eddy Current in MFL Type NDT," *IEEE Transactions on Magnetics*, Vol. 40, No. 2, pp. 663–666.

Ramuhalli, P., L. Udpa, and S.S. Udpa, 2003, "Neural Network-Based Inversion Algorithms in Magnetic Flux Leakage Nondestructive Evaluation," *Journal of Applied Physics*, Vol. 93, pp. 8274–8276.

Shcherbinin, V., and A. Pashagin, 1972, "Influence of the Extension of a Defect on the Magnitude of its Magnetic Field," *Defektoskopiya*, Vol. 8, No. 4, pp. 84–78.

Shi, P. P., 2015, "Analytical Solutions of Magnetic Dipole Model for Leakage Magnetic Fields," *Nondestructive Testing*, Vol. 37, No. 3, pp. 1–7.

Sun, Y. H., S. W. Liu, Z. J. Ye, S. Chen, and Q. Zhou, 2016, "A Defect Evaluation Methodology Based on Multiple MFL Testing Signal Eigenvalues," *Research in Nondestructive Evaluation*, Vol. 27, No. 1, pp. 1–25.

Tumanski, S., 2007, "Induction Coil Sensors—A Review," *Measurement Science and Technology*, Vol. 18, No. 3, pp. R31.

Wang, P., Y. Gao, G.Y. Tian, and H. Wang, 2014, "Velocity Effect Analysis of Dynamic Magnetization in High Speed Magnetic Flux Leakage Inspection," *NDT & E International*, Vol. 64, pp. 7–12.

Wu, J., H. Fang, X. Huang, H. Xia, Y. Kang, and C. Tang, 2017, "An Online MFL Sensing Method for Steel Pipe Based on the Magnetic Guiding Effect," *Sensors*, Vol. 17, No. 12, p. E2911.

Wu, J., H. Fang, L. Li, and Y. Kang, 2016, "The Signal Characteristics of Rectangular Induction Coil Affected by Sensor Arrangement and Scanning Direction in MFL Application," *International Journal of Applied Electromagnetics and Mechanics*, Vol. 52, Nos. 3–4, pp. 1257–1265.

Wu, J., Y. Sun, B. Feng, and Y. Kang, 2017, "The Effect of Motion-Induced Eddy Current on Circumferential Magnetization in MFL Testing for a Steel Pipe," *IEEE Transactions on Magnetics*, Vol. 53, No. 7, doi: 10.1109/TMAG.2017.2655483.

Wu, J., Y. Sun, Y. Kang, and Y. Yang, 2015, "Theoretical Analyses of MFL Signal Affected by Discontinuity Orientation and Sensor-Scanning Direction," *IEEE Transactions on Magnetics*, Vol. 51, No. 1, doi: 10.1109/TMAG.2014.2350460.

Xu, J., X. Wu, C. Cheng, and A. Ben, 2012, "A Magnetic Flux Leakage and Magnetostrictive Guided Wave Hybrid Transducer for Detecting Bridge Cables," *Sensors*, Vol. 12, No. 1, pp. 518–533.

Zatsepin, N., and V. Shcherbinin, 1966, "Calculation of Magneto Static Field of Surface Defects. I. Field Topography of Defects Model," *Defektoskopiya*, Vol. 50, No. 5, pp. 50–59.

Zeng, Z., L. Xuan, Y. Sun, L. Udpa, and S. Udpa, 2004, "Probability of Detection Model for Gas Transmission Pipeline Inspection," *Research in Nondestructive Evaluation*, Vol. 15, No. 3, pp. 99–110.

Zhang, D., M. Zhao, and Z. Zhou, 2012, "Quantitative Inspection of Wire Rope Discontinuities Using Magnetic Flux Leakage Imaging," *Materials Evaluation*, Vol. 70, No. 7, pp. 872–878.